CrossMark

Enhancement of SO$_2$ gas sensing performance using ZnO nanorod thin films: the role of deposition time

Brian Yuliarto[1,2,*] (iD), Muhammad Fazri Ramadhani[1], Nugraha[1], Ni Luh Wulan Septiani[1], and Kholoud Ahmed Hamam[3]

[1] *Advanced Functional Materials Laboratory, Engineering Physics Department, Institut Teknologi Bandung, Bandung, Indonesia*
[2] *Research Center for Nanosciences and Nanotechnology, Institut Teknologi Bandung, Bandung, Indonesia*
[3] *Department of Physics, King Abdulaziz University, Jeddah, Saudi Arabia*

ABSTRACT

In this study, a sensor with a controllable thin film of zinc oxide (ZnO) nanostructures with different deposition times is successfully synthesized over alumina substrates by chemical bath deposition methods. The seed of ZnO is grown using the dip-coating method, and ZnO thin film is grown by chemical bath deposition (CBD) using the precursor of $Zn(NO_3)_2 \cdot 4H_2O$. Chemical bath deposition was done three times to investigate the role of deposition time toward gas sensing properties. Structure, morphology, and composition of the ZnO thin films are characterized using X-ray diffraction, scanning electron microscopy, and energy dispersive spectroscopy, respectively. From the morphology characterization, the ZnO nanostructure from two-times CBD and three-times CBD process shows different sizes and densities of nanorods compared to the ZnO thin film from one-time CBD process. Increasing thickness of thin film is also observed in two-times CBD of ZnO. The gas sensor characterization test results show that the ZnO thin films from two-times CBD can improve the sensing response to be 93% for SO$_2$ gas at 70 ppm of concentration at working temperature of 300 °C, which is an increase of 15% compared to ZnO thin films from one-time CBD. At different operation temperatures, the response of two-times CBD ZnO nanorod increases 20–40% over one-time CBD ZnO nanorod. The three-times CBD ZnO nanorod showed non-order and high-density nanostructure yielding low resistance value and cause low sensor response.

Address correspondence to E-mail: brian@tf.itb.ac.id

Springer

Introduction

Recently, greenhouse gas emissions from fossil fuel combustion have caused major pollution problems, forcing environmental researchers to concentrate their efforts on overcoming such problems. Sulfur dioxide (SO_2) is one of the most hazardous pollutants for human health and the atmosphere [1, 2]. The most significant anthropogenic emission sources of SO_2 gas are the combustion of sulfur-containing fossil fuels, smelting sulfide ores, petroleum refining, and volcanic smoke [3–5]. Moreover, other less significant sources include chemical and industrial process, allied products manufacturing, industrial processes, metal processing, and vehicle emissions [6]. Exposure to SO_2 gas may cause immediate bronchial constriction, narrowing of the airways, increased pulmonary resistance, and possibility of increased airway reactivity [5]. Given these dangers, it is urgently necessary to create accurate monitoring of SO_2 concentration. SO_2 gas monitoring applications need sensors and data acquisition systems that detect the presence of SO_2 gas in any concentration. Moreover, high performance SO_2 sensors that increase the accuracy and reliability of the monitors are highly sought after.

Recently, semiconductor nanostructures have attracted interest for use in sensor materials, specifically as potential system devices for high performance nanoelectronics. Among them, zinc oxide (ZnO) has proved to be one the most promising materials for various applications, including gas sensors. ZnO is a metal oxide semiconductor material that has a wide band gap (3.3 eV), high exciton binding energy around 60 meV, with wurtzite crystal structure and piezoelectric properties [7–9]. These unique properties have potential for use in various sensors and actuators [10]. The sensitivity of gas sensor materials largely depends on the amount of gas adsorbed on the material's surface. In recent development of sensor materials, the nanostructure modifications have yielded better sensing performance [11–13]. One technique in the improvement of sensing performances is to increase the interactive specific surface layer of the sensor material by constructing nanostructure metal oxides, resulting in enhanced sensitivity through more depletion of the absorbed carrier trapped on the surface of the nanostructure. Efforts have been directed at fabricating one-dimensional (1D) nanostructures, such as nanowires, nanorods, nanotubes, or nanosheets because of their unique physical and chemical properties [14, 15]. The controlled synthesis of multidimensional semiconductors has attracted much attention due to their unique structure and morphology, which provides a higher surface to volume ratio [16], so they can absorb more gas.

Moreover, the ZnO nanostructure can be prepared or synthesized using various methods that yield different morphologies such as nanowires, nanobelts, nanotubes, nanorings, nanosprings, and nanohelices [17, 18]. By manipulating the nanostructure of ZnO, the sensitivity of ZnO as part of a gas sensor can be enhanced [19–22]. However, the role of deposition time of ZnO toward gas sensing properties has not been reported according to our knowledge. Taking advantage of the increased access between environmental SO_2 and a nanostructure of the sensor's sensitive layer [23], we have prepared the nanostructure of ZnO with different deposition times to know the role of deposition time and to create a better sensing performance for SO_2 gas detection. In this paper, we report on the fabrication of a novel modified nanostructure of ZnO using the repeated chemical bath depositions technique. The different deposition times of ZnO nanostructure yields ZnO nanostructure thin film with short nanorods, long nanorods, and double-layer nanorods depend on how many depositions have been performed. The higher surface area of ZnO long nanorod from two-times CBD ZnO nanorod should yield better access for the target gas to make a reaction on the sensitive layer of ZnO thin film. Compared to the ZnO short nanorod, the long-rod ZnO thin film can improve the sensing performance of the ZnO for the SO_2 gas. Subsequently, the sensing properties and response of this long-nanorod ZnO sensor for SO_2 gas are investigated, and they confirm improvement in the sensor's performance.

Experimental

Materials

The precursors that were used in this study are Zinc Acetate tetrahydrate ($Zn(CH_3COO)_2 \cdot 4H_2O$), Zinc Nitrate hexahydrate ($Zn(NO_3)_2 \cdot 6H_2O$), Hexa Methyl Tetra Amine (HMTA), Diethanol Amine (DEA), and Ethylene Di Amine (EDA). The solutions that were used as solvents are Ethylene Glycol, Ethanol, and DI
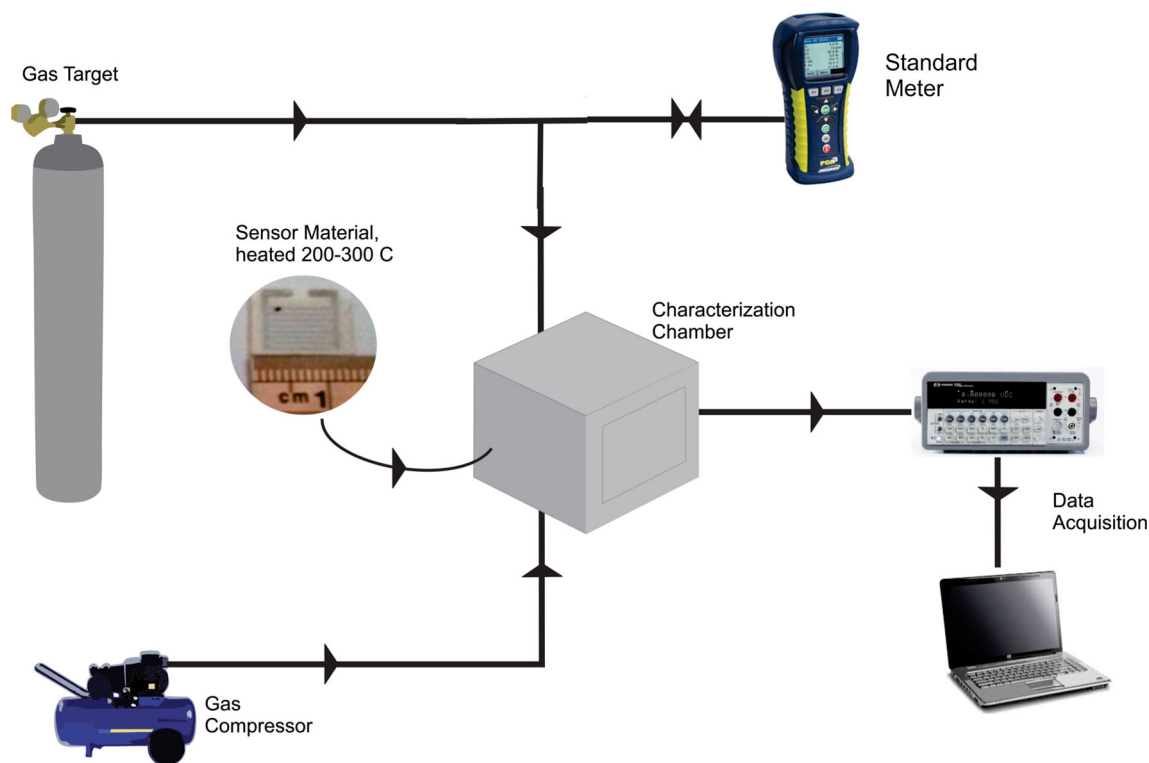
**Figure 1** Schematic diagram of the apparatus for SO_2 gas sensing characterization.

water. All chemicals were of analytical grade and used without further purification. Alumina (Al_2O_3) is used as a substrate for the sensor devices in this study. The substrates were cleaned with soap, ethanol, and distilled water using ultrasonic cleanser. For the synthesis process of the ZnO nanorod structure, the simple cylindrical glasses with a controllable heater were used.

Synthesis methods

First, the silver electrode is prepared on the alumina substrate. The silver inter-digitated array electrode having finger gap at 0.5 mm was deposited onto alumina substrate by screen printing method, and was dried at 400 °C for 30 min. In a typical reaction, 0.2 M $Zn(CH_3COO)_2\cdot4H_2O$ was dissolved in 60 ml of Ethylene Glycol and then Diethanol Amine (DEA) was added into the mixture solution. The mixture solution was stirred at 70° C for 30 min, and the resulting solutions were cooled to room temperature. The substrate then underwent a dip-coating process for two times using the resulting mixture solution for 10 s. The speed of dip coating was 0.05 cm/s. The deposited thin films were dried at 120 °C for 15 min,

and continued in calcination at 450 °C for 30 min to yield the ZnO seed. A solvent for the first Chemical Bath Deposition (CBD) process prepared by adding 0.015 M of $Zn(NO_3)_2\cdot6H_2O$ into 60 ml solution consisting of DI water and ethanol (the mol composition of DI water:ethanol is 3:1). After 30 min of stirring, 0.02 M of the HMTA was added into the mixture solution and stirred once again for 30 min. After that, this resulting solution was added by EDA and stirred once again for 30 min. The Al_2O_3 substrate, with the ZnO seed at the surface from the first process of dip coating, was immersed into this solution 90 °C for 1 h to get one-time CBD sample. The resulting substrate with the short nanorods was then dried in room temperature and immersed into ethanol and calcinated for 1 h at 450 °C.

For the two-times CBD and three-times CBD samples, a solvent for the CBD process was prepared by adding 0.02 M of $Zn(NO_3)_2\cdot6H_2O$ into 60 ml solution consisting of DI water and ethanol (the mol composition of water:ethanol is 3:1). After 30 min of stirring, 0.02 M of HMTA was added into the mixture solution. This solution was mixed for another 30 min. After that, this resulting solution was added by EDA and stirred once again for 30 min. Al_2O_3 substrates
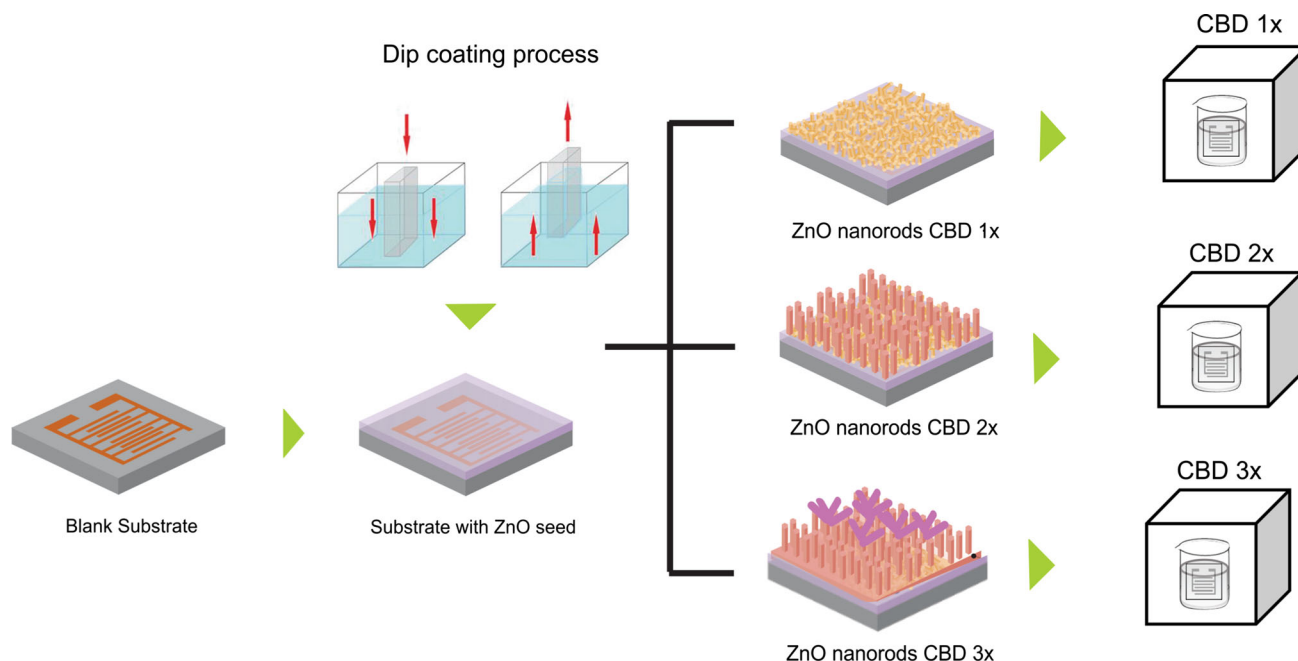
Figure 2 Step by step of deposition process for ZnO nanorod thin films to fabricate one-time CBD, two-times CBD, and three-times CBD.

with ZnO nanostructures thin film from one-time CBD were immersed into the solution for 16 h at 90 °C to get two-times CBD sample. After that, the films were dried at room temperature and immersed into the ethanol and calcinated for 1 h at 450 °C. For the three-times CBD process, the second CBD process was repeated, and after the second calcinations, the Al_2O_3 substrates with ZnO nanostructure thin film from two-times CBD were immersed again into the solution for another 16 h at 90 °C to get three-times CBD samples.

The crystal structure of the resulting thin films was determined by X-ray diffraction (XRD) using a Philips Analytical X-ray with diffraction pattern of CuKa radiation ($\lambda = 1.54060$ Å) through 40 kV generators and 25 mA current. The machine is set to step scan mode with step size at 0.020 and step time at 0.5 s for each 2θ (20°–90°). The surface morphologies of the thin films prepared for the seed only layer, one-time CBD, two-times CBD, and three-times CBD are observed by scanning electron microscopy (SEM) using JEOL-JSM-6510 LV. Moreover, the sensor performance characterizations are tested using the sensor system as shown in Fig. 1. Figure 1 describes the gas sensor characterization apparatus, which comprised primarily of a gas target supplier, mass flow controller, standard measurement, and the test

characterization chamber where the sample was put inside. The sensor sample was installed in the test characterization chamber and connected to the voltage unit via data acquisition systems. The sensor response was measured in the presence of SO_2 at various temperatures to discern the best operation temperature for the sensors.

Results and discussion

The detailed deposition process of ZnO nanostructure is shown in Fig. 2. The ZnO seed layer was grown on the substrate using the dip-coating technique. Subsequently, one-time CBD, two-times CBD, and three-times CBD were deposited onto ZnO seeds alumina substrate using the chemical bath deposition method. The resulting ZnO, consisting of different types nanorod structures, was observed as an SO_2 gas sensor at various concentrations. The gas sensing properties of different sensor thin films were tested in the presence of SO_2 and ambient air at certain working temperature. The sensor performances of the seed ZnO thin films were also tested as comparisons.
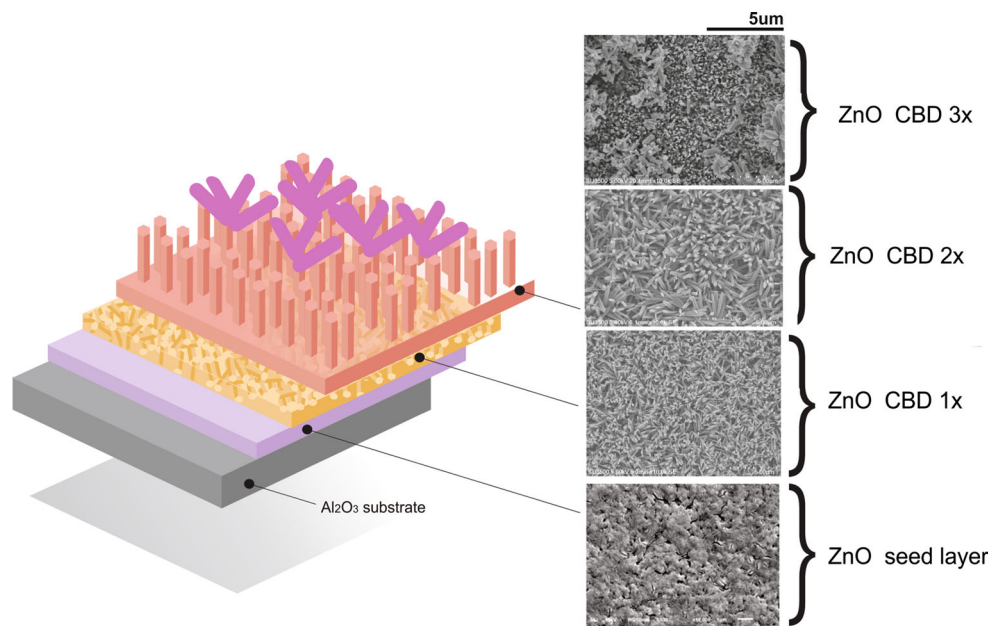
The XRD results from samples of one-time CBD, two-times CBD, and three-times CBD on the alumina (Al_2O_3) substrates were investigated after the CBD

process and calcination at a temperature of 450 °C. The XRD results of one-time CBD, two-times CBD, and three-times CBD are shown in Fig. 3. The XRD measurement results show that the phase formed by one-time CBD, two-times CBD, and three-times CBD of ZnO nanorod thin films are clearly polycrystalline ZnO with diffraction peaks that can be indexed mainly to the hexagonal wurtzite ZnO. The nanorods effect for two-times CBD and three-times CBD is shown in Fig. 3. It is clear that both nanorods have a higher intensity and sharper peak compared to the
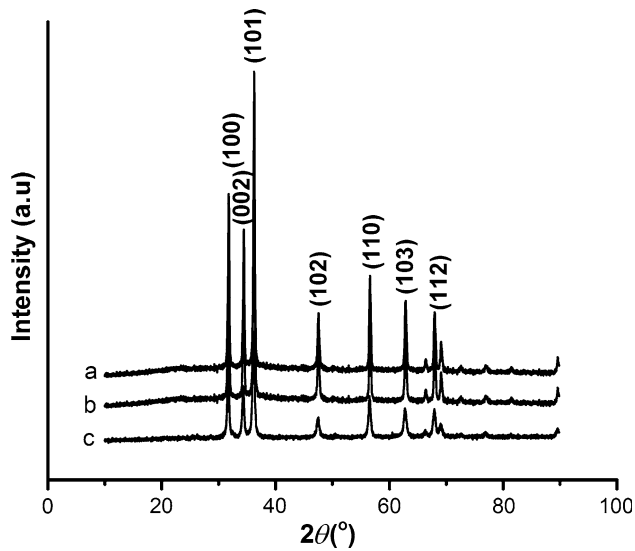

Figure 3 The diffraction pattern of ZnO nanorod thin films from three-times CBD (*a*), two-times CBD (*b*), and one-time CBD (*c*).

nanorods from one time CDB. The higher intensity of the peak from two-times CBD and three-times CBD of ZnO nanorod thin film indicates more order of the phase structure from their longer nanorods and thicker layer.

The upside SEM micrographs of the seed layer, one-time CBD, two-times CBD, and three-times CBD of ZnO thin films are shown in Fig. 4. The SEM results for the ZnO seed layer samples have pattern of regular granule morphology. Based on Fig. 4, the rods did not formed on seed layers. The rods started forming on the one-time CBD process. The density of the rods from two-times CBD is higher than the density of one-time CBD ZnO nanorod thin film. Moreover, after three-times CBD, the new nanorod structure is grew above the layer of two-times CBD nanorod layer and formed as second layer nanorods. The morphology pattern of the long nanorods ZnO thin film shows that the long nanorod structures are more ordered compared to the short ZnO nanorods. The cross section SEM image of the comparison of seed layer, one-time CBD, two-times CBD, and three-times CBD is shown in Fig. 5. The SEM results on Fig. 5 show that the seed layer is very thin with the thickness about 150 nm. The one-time CBD of ZnO thin film has short rod size. The two-times CBD has bigger and longer ZnO nanorod compared to that of one-time CBD, while the three-times CBD has double layer and non-order nanorod structure of ZnO. The comparison of the thickness of ZnO nanorods at

Figure 4 The SEM of layer by layer of ZnO nanorod thin films in different times of deposition.
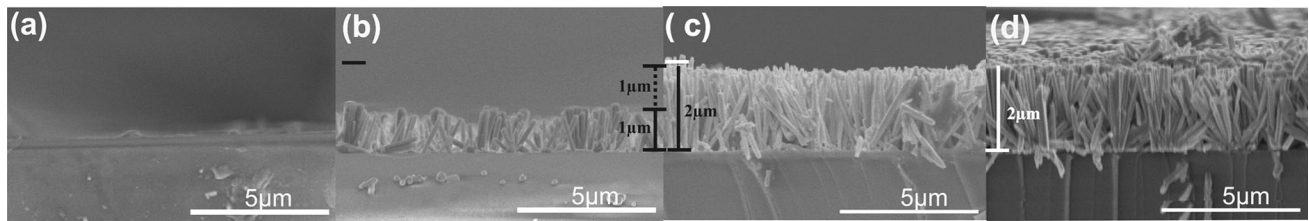
Figure 5 The cross section SEM of ZnO nanorod thin films for seed layer (**a**), one-time CBD (**b**), two-times CBD (**c**) and three-times CBD (**d**).
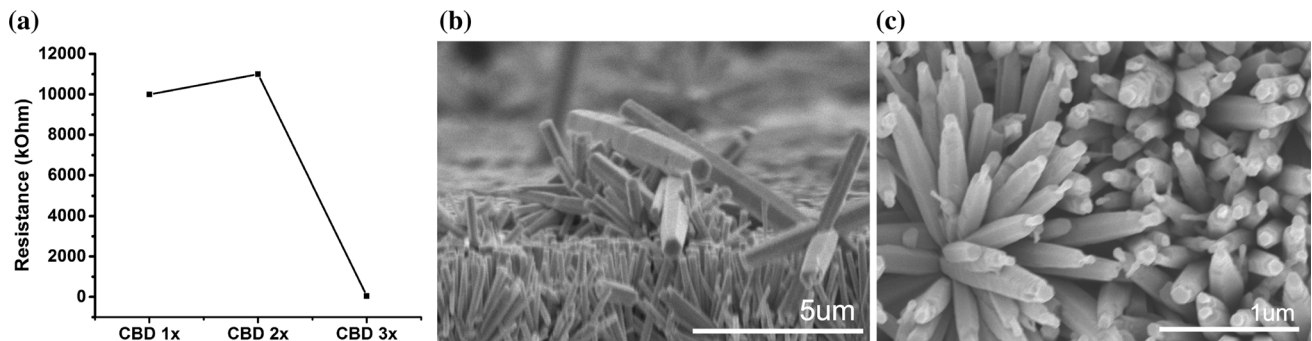

Figure 6 Electrical properties of one-time CBD, two-times CBD, and three-times CBD (**a**), cross section SEM image of three-times CBD ZnO nanorod thin film (**b**), and top view of FE SEM image of double layer nanorod of three-times CBD ZnO nanorods thin film (**c**).

different deposition times is shown in Fig. 5. The nanorod of one-time CBD is short and the thickness is about 1 μm. The second process permitted ZnO to continue to grow on the first rods so that the thin film thickness increased significantly to be 2 μm. However, when the three-times CBD deposition is performed, it seems that no increasing rod was observed. In the case of three-times CBD, the second layer of ZnO nanorod was formed to yield double layer and more multi-junction joint structure of ZnO nanostructure as shown in Fig. 6.

To know the electrical properties of all samples, the resistances of each thin film ZnO nanostructure samples were measured at 300 °C. The resistance of one-time CBD, two-times CBD, and three-times CBD are 10000, 11000, and 50 kΩ, respectively, as shown in Fig. 6a. It is clear that the resistance of ZnO nanostructure thin film decreases significantly at three-times CBD. This phenomenon is yielded by the existence of double layers nanorods that create multi-junction joints at each nanorods as shown in Fig. 6b. Therefore, the contacts between each nanorods form electron accumulation layer which leads to the decrease in resistance [24]. The low resistance of three-times CBD affects its dynamic response to the SO₂ gas exposure. Moreover, the nanorod pattern

was confirmed from upside SEM image that there is no hollow in the structure as shown in Fig. 6c. This typical non-hollow nanorod structure actually has been observed in other studies prepared by similar methods [15].

The resulting ZnO nanostructure thin films were characterized for their sensing performance in terms of their response towards SO_2 gas. The silver electrodes were printed on the surface of Alumina substrate before the synthesis process for the growth of ZnO nanostructure thin films. As the sensor devices were placed in the characterization chamber, the chamber was heated to a certain temperature and controlled by a PID temperature controller. The seed, one-time CBD, and two-times CBD of ZnO nanorod thin films were investigated to determine the sensing performance of SO_2 gas. Each of the samples has been tested for five times to make sure that the data are valid. The dynamic responses of the samples give an overview of the value of the resistance that occurs with respect to the time of testing. The response of the sensor was calculated using Eq. (1), where R is sensor response; Ra is the resistance at air conditions, and Rg is the resistance at target gas conditions. Moreover, the sensitivity of the sensor (S) was defined as the transient number of the gas response.
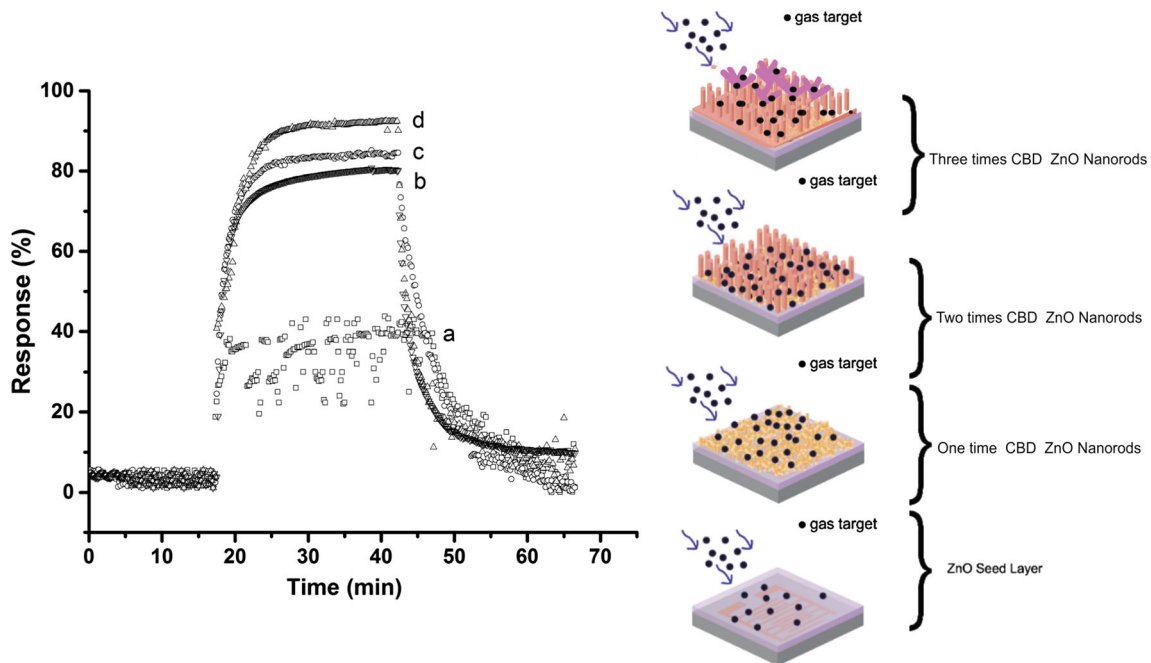
Figure 7 The sensor response after exposure of 70 ppm SO$_2$ gas for seed layer (*a*), one-time CBD (*b*), two-times CBD (*c*), and three-times CBD (*d*) of ZnO nanorod thin films at the temperature of 300 °C.

$$R = \frac{R_a - R_g}{R_a} \cdot 100\%. \tag{1}$$

The sensor's response of all samples after the SO$_2$ gas exposure of 70 ppm at 300 °C is shown in Fig. 7. The sensor response increases from ZnO seed layer to two-times CBD ZnO nanorod structure, and after that the sensor response decreases on three-times CBD ZnO nanostructure. Due to the low resistance value of three-times CBD ZnO nanorod sample, the resistance changes of the sensor prior to exposure to the SO$_2$ gas could not be significantly observed, thus leading to a low sensor response. This phenomenon is consistent with the barrier potential theory. The barrier potential is actually formed in between two or more rods that in contact [19], which could block electron transport. When this was exposed to the air, oxygen adsorption increased the barrier's presence. In the presence of SO$_2$ or reductive gas, gas molecule reacted with oxygen ions to yield SO$_3$ and release the electron back into the conduction band. It caused the depletion layer to become narrow and decrease the barrier potential, allowing electrons to move easily [25–27]. The easy movement of electron in three-times CBD nanorods ZnO thin films yields low resistance value and low sensor response. Moreover, its low sensor response will make this type of sensor

will not be further investigated for other sensor properties.

Figure 8 shows the sensor sample's typical dynamic response for both one-time CBD and two-times CBD ZnO nanorod thin films for the exposure of the SO$_2$ gas at several different operation temperatures. The two-times CBD ZnO nanorod sensor shows a higher response compared to the one-time CBD ZnO nanorods at operation temperatures of 200, 250, and 300 °C. The detail data of sensor response, time response, and time recovery are shown in Table 1. It can be seen that the response sensor of two-times CBD ZnO thin films has higher sensor response at about 15, 20, and 40% than that of one-time CBD ZnO thin films at working temperatures of 300, 250, and 200 °C, respectively. The response of both sensors increases as the concentration of SO$_2$ gas in contact with the sensors increases. It is also shown in Fig. 8 that the response of the sensors increases with increasing operation temperature. When temperature increases, O$_2$ has more energy to adsorb on the surface of ZnO, so there is more O$^-$ on the sensor surface causing increased reactions between SO$_2$ and O$^-$, which increases the sensor response. But above 300 °C, the resistance of the sensor tends to decrease to the very small value, which leads to decrease the

Figure 8 The dynamic response of the sensor at various temperatures (**a**), and sensor response as a function of temperature (**b**) after the exposure of 70 ppm SO₂ gas for the one-time CBD and two-times CBD thin films.
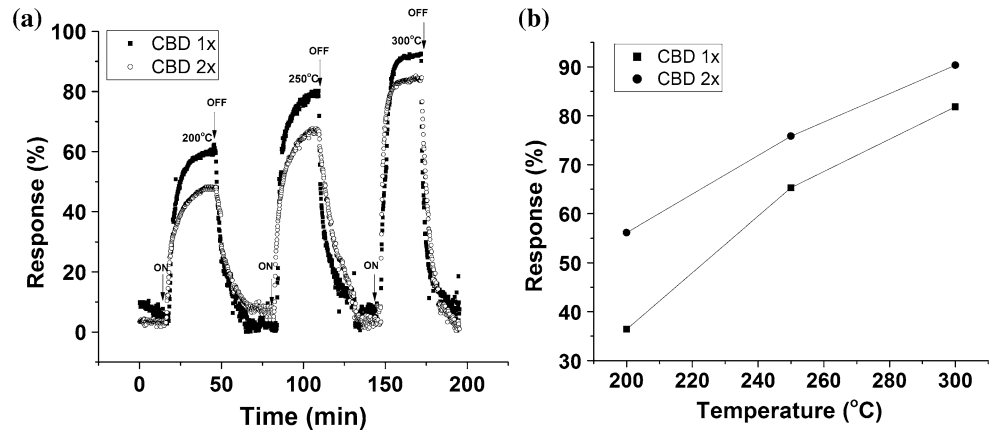
Table 1 Response data of one-time CBD and two-times CBD of ZnO thin films toward 70 ppm SO₂ gas

T (°C)	Response (%)		$t_{response}$ (min)		$t_{recovery}$ (min)	
	CBD 1×	CBD 2×	CBD 1×	CBD 2×	CBD 1×	CBD 2×
200	41	59.2	12.8	21	13.5	8
250	67	80	11	10	22	8
300	81	93	6	5.8	10.8	4.6

Figure 9 FE SEM images and modeling the active layer density of ZnO nanorods from one-time CBD and two-times CBD.

CBD 1x d= 106.47 nm

CBD 2x d = 165.78 nm
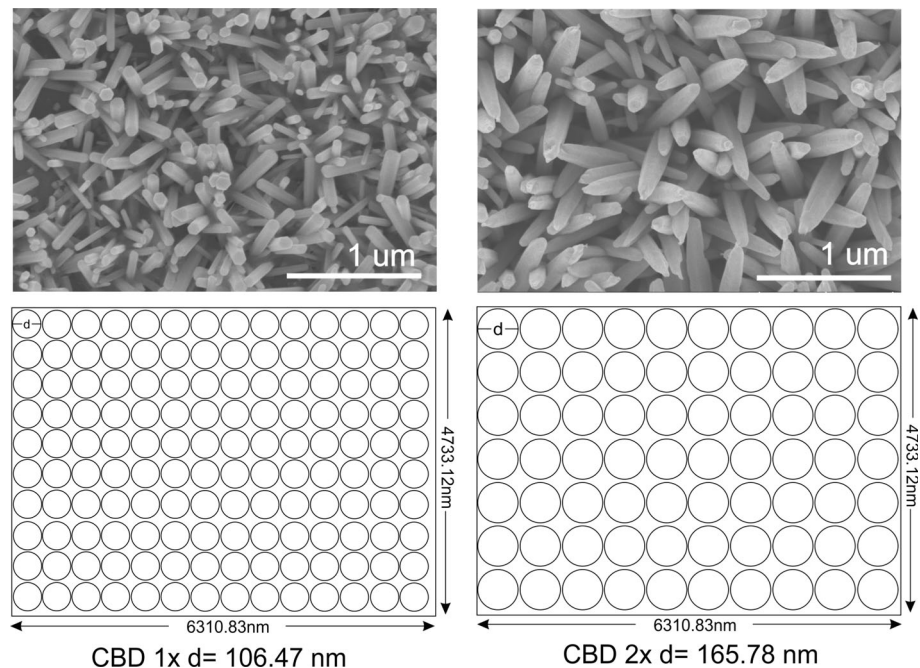
sensor response [28]. Thus, we can conclude that the optimum working temperature for SO₂ sensors is 300 °C. Moreover, the two-times CBD ZnO showed better response at all operating temperatures compared to that of one-time CBD ZnO as shown in Fig. 8. This indicates that the higher changing of resistance happened on the surface of nanorods from two-times CBD ZnO which is different with that on the one-time CBD ZnO. This phenomenon can be explained by comparing the density of active layer on ZnO nanorod thin films.

$$\text{Density active site} = n \cdot \pi r^2 t \qquad (2)$$

To know the active layer density of the ZnO nanorods, we modeled the ZnO nanorods on a certain square of substrate with the assuming that the nanorod is well ordered. Figure 9 shows FE SEM images and the model of active layer nanorods from one-time CBD and two-times CBD. From Fig. 9, it can be defined that the diameters of one-time CBD and two-times CBD are 106.47 nm and 165.78 nm, respectively. The three-times CBD is not included in model because the resistance of ZnO nanorods is very small compared to that of one-time CBD and two-times CBD. From the model, the active layer density can be calculated by Eq. (2), where n is number of rod; r is radius of rod, and t is the length of rod. According to the described model, it can be calculated that the number of rods in the certain SEM space of one-time CBD and two-times CBD is 3356 rods and 1384 rods, respectively. If we consider the height of rods from the SEM as shown in Fig. 5 and the number of rods as described in the model, we can get the density as a function of nanorods volume times the number of nanorods (Eq. 2) as shown in Table 2. It is shown in Table 2 that the active layer density of two-times CBD is 58.44 which is more than two times than that of one-time CBD.

Table 2 The active layer properties of ZnO nanorods from one-time CBD and two-times CBD at 29.87 mm^2

	r rods (μm)	n rod	t (μm)	Density (vol unit)
CBD 1×	0.053	3356	1	26.34
CBD 2×	0.082	1384	2	58.44

The increasing response of the longer nanorod resulted from two-times CBD can be explained by considering the depletion layer theory. The depletion layer is formed on the surface of ZnO nanorods. According to the depletion theory, at certain temperature, oxygen ions are chemisorbed to the surface of nanorods: taking an electron from the conduction layer, and creating a depletion layer on the surface. In the case of the one-time CBD of ZnO nanorod thin films, the depletion layer only formed on the surface of ZnO nanorods [29]. When the surface is exposed to SO$_2$ gas, width of depletion layer decreased while the electron conduction path, or conductance of ZnO increased as shown in Fig. 10 [18]. As a result, the sensor resistance decreases upon the exposure to SO$_2$ gas. In case of two-times CBD of ZnO nanorods thin
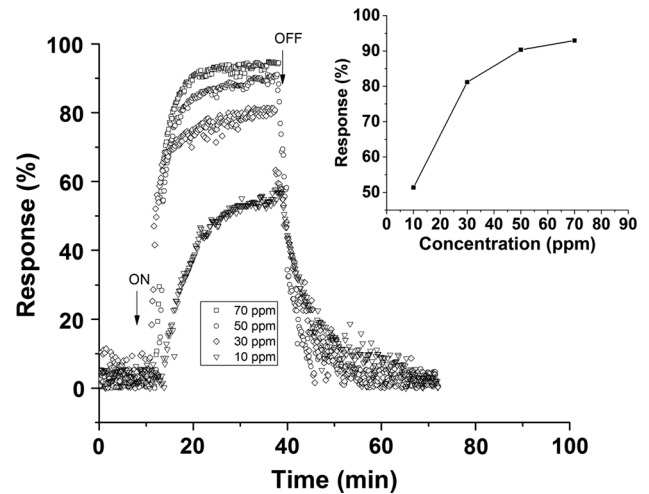
Figure 11 The sensitivity of the long nanorods of ZnO nanostructure thin films at 300 °C.
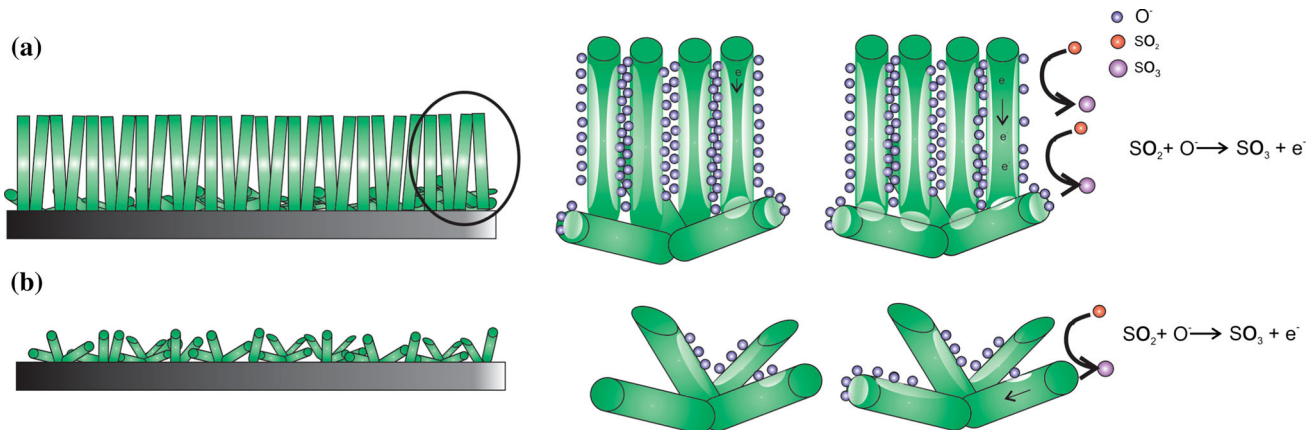
Figure 10 The illustration of the sensing mechanism on the exposure of SO$_2$ gas on the surface of two-times CBD of ZnO nanorod thin films (**a**) and one-time CBD of ZnO nanorod thin films (**b**).

Figure 12 Stability gas two-times CBD of ZnO toward 70 ppm at 300 °C on 1st, 7th, 14th days, and 1 month (**a**), and SO$_2$ gas selectivity of long nanorod of ZnO toward CO gas (**b**).
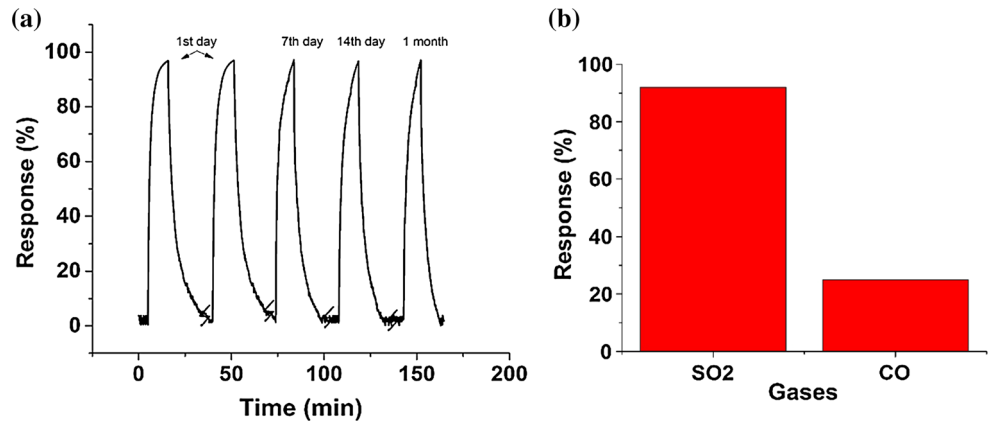
films, the longer nanorods would yield much oxygen into the surface wall of the rods so that the SO$_2$ gas exposure can increase the width of depletion layer and finally increase the sensor response. This phenomenon is consistent with the previous explanations about comparison of active layer density between one-time CBD and two-times CBD. Table 2 shows that the active layer density of two-times CBD ZnO nanorod thin film is higher than the active layer density of one-time CBD ZnO nanorod thin films.

The two-times CBD sensor's response to different concentrations of SO$_2$ gas is shown in Fig. 11. It clearly shows that the response sensor increases with an increase in SO$_2$ concentration from 10 to 70 ppm. The heightened response from 10 to 70 ppm of SO$_2$ gas is explained by diffusion theory, which states that diffusion rate or adsorption rate increases as the gradient concentration increases. This causes the surface reaction to become faster and the response time to decrease [30]. The measurements show that at a 10 ppm concentration of SO$_2$, the long ZnO nanorod sensors can yield slow response. Moreover, it is shown at the inset of Fig. 11 that at 70 ppm concentration of SO$_2$, the ZnO surface starts to saturate because the whole surface has reacted with gasses so the response will remain the same despite the increase in SO$_2$ concentration.

$$\text{Selectivity of SO}_2 = \frac{R_{\text{SO}_2}}{R_{\text{SO}_2} + R_{\text{CO}}}. \tag{3}$$

The detail data of time response and time recovery of the sensors at an SO$_2$ concentration of 70 ppm are presented in Table 1. For both one-time CBD and two-times CBD nanorods of ZnO thin films, almost all time response and time recovery decreases with increasing temperature. When temperature increases,

the SO$_2$ has more energy and become more energetic, so the reaction time decreases. Moreover, time response and recovery of two-times CBD of ZnO thin films is shorter than that of one-time CBD of ZnO because the long nanorods of ZnO two-times CBD provide more diffusion paths than the short one, so the reaction between the gas and the surface is faster. To evaluate the sensor's stability and repeatability, the sensor response of two-times CBD at an SO$_2$ concentration of 70 ppm and a temperature of 300° C was performed. The sensor response was measured during certain periods on the one day, seventh day, fourteenth day, and after one month as shown in Fig. 12. This stable performance shows that the sensor has good durability during certain time of usage. The sensor's response values remain the same but the response time seems to take longer with more time. But, these differences are relatively small because the sensor has good repeatability. Additionally, the two-times CBD ZnO nanorod thin film has lower response to CO gas than to SO$_2$ gas (Fig. 12). The selectivity property of long ZnO nanorods is shown by the formula in Eq. (3) [31]. For SO$_2$ and CO, the selectivity of ZnO nanostructure is 0.82 and 0.18, respectively. This means the two-times CBD ZnO nanorod thin film has high selectivity towards SO$_2$ gas compared to CO gas.

Conclusions

Our experiment tests the synthesis of the different lengths of nanorods of ZnO thin films as the surface material for SO$_2$ gas sensors. The ZnO nanorod structure thin films were successfully fabricated using the triple-stage Chemical Bath Deposition

(CBD method). The CBD technique was performed one to three times using Zinc $(CH_3COOH)_2 \cdot 4H2O$ and $Zn(NO_3) \cdot 4H_2O$ with the addition of HMTA and EDA. XRD results showed that the two-times CBD of ZnO thin films has better crystallization than short nanorods of ZnO thin films. The ZnO nanorod created from one-time CBD has short nanorod structure, while the ZnO nanorod created from two-times and three-times CBD process has longer nanorod and larger diameter. The two-times CBD of ZnO thin films shows higher response in all various concentrations of SO_2 gas compared to the one-time CBD ZnO nanorods thin film. The gas sensor characterization test results show that the two-times CBD of ZnO improves sensor response to 93% for SO_2 gas at a concentration of 70 ppm and temperature of 300° C, which is an increase of 15% over the one-time CBD ZnO nanorods thin films. At different operation temperatures, the response of two-times CBD ZnO nanorods increases 20–40% over the one-time CBD of ZnO nanorods. Additionally, the sensor response increases as the concentration of SO_2 increases from 10 to 70 ppm. These results show that longer ZnO nanorods will increase the performance of SO_2 gas sensing, and are a better choice for accurate and reliable gas-sensing devices.

Acknowledgements

References

[1] Tyagi P, Sharma A, Tomar M, Gupta V (2016) Metal oxide catalyst assisted SnO_2 thin film based SO_2 gas sensor. Sens Actuat B 224:282–289. doi:10.1016/j.snb.2015.10.050

[2] Liu F, Wang Y, Wang B, Yang X, Wang Q, Liang X, Sun P, Chuai X, Wang Y, Lu G (2017) Stabilized zirconia-based mixed potential type sensors utilizing $MnNb_2O_6$ sensing electrode for detection of low-concentration SO_2. Sens Actuat B 238:1024–1031. doi:10.1016/j.snb.2016.07.145

[3] Lee SC, Hwang BW, Lee SJ, Choi HY, Kim SY, Jung SY, Ragupathy D, Lee DD, Kim JC (2011) A novel tin oxide-based recoverable thick film SO_2 gas sensor promoted with magnesium and vanadium oxides. Sens Actuat B 160:1328–1334. doi:10.1016/j.snb.2011.09.070

[4] Li H, Wang Q, Xu J, Zhang W, Jin L (2002) A novel nano-Au-assembled amperometric SO_2 gas sensor: preparation, characterization and sensing behaviour. Sens Actuat B 87:18–24. doi:10.1016/S0925-4005(02)00189-2

[5] Liang X, Zhong T, Quan B, Wang B, Guan H (2008) Solid-state potentiometric of SO_2 sensor combining NASICON with V_2O_5-doped TiO_2 electrode. Sens Actuat B 134:25–30. doi:10.1016/j.snb.2008.04.003

[6] Das S, Rana S, Mursalin SkMd (2015) Sonochemically prepared nanosized $BiFeO_3$ as novel SO_2 sensor. Sens Actuat B 218:122–127. doi:10.1016/j.snb.2015.04.084

[7] Moezzi A, McDonagh AM, Courtie MB (2012) Zinc oxide particles: synthesis, properties and applications. Chem Eng J 185:1–22. doi:10.1016/j.cej.2012.01.076

[8] Djuriscic AB, Chen X, Leung YH, Ching Ng AM (2012) ZnO nanostructures: growth, properties and applications. J Mater Chem 22:6526–6535. doi:10.1039/C2JM15548F

[9] Lehraki N, Aida MS, Abed S, Attaf N, Attaf A, Poulain M (2012) ZnO thin films deposition by spray pyrolysis: influence of precursor solution properties. Curr Appl Phys 12:1283–1287. doi:10.1016/j.cap.2012.03.012

[10] Galstyan V, Comini E, Baratto C, Faglia G, Sberveglieri G (2015) Nanostructured ZnO chemical gas sensors. Ceram Int 41:14239–14244. doi:10.1016/j.ceramint.2015.07.052

[11] Yamada T, Katsumura Y, Yuliarto B, Chihara M, Zhou H, Honma I (2004) Effect of tin addition on mesoporous silica thin film and its application for surface photovoltage NO_2-gas sensor. Anal Chem 22:6719–6726. doi:10.1021/ac0495642

[12] Yuliarto B, Honma I, Katsumura Y, Zhou H (2006) Preparation of room temperature NO_2 gas sensors based on W- and V-modified mesoporous MCM-41 thin films employing surface photovoltage technique. Sens Actuat B 114:109–119. doi:10.1016/j.snb.2005.04.016

[13] Yuliarto B, Nulhakim L, Ramadhani MF, Iqbal M, Nugraha, Suyatman, Nuruddin A (2015) Improved Performances of Ethanol Sensor Fabricated on Al-Doped ZnO Nanosheet Thin Films. IEEE Sens J 15:4114–4120. doi:10.1109/JSEN.2015.2410995

[14] Yuliarto B, Julia S, Septiani NLW, Iqbal M, Ramadhani MF, Nugraha (2015) The effect of tin addition to ZnO nanosheet thin films for ethanol and isopropyl alcohol sensor applications. J Eng Technol Sci 47:76–91. doi:10.5614/2Fj.eng.technol.sci.2015.47.1.6

[15] Zhang H-D, Long Y-Z, Li Z-J, Sun B (2014) Fabrication of comb-like ZnO nanostructures for room-temperature CO gas sensing application. Vacuum 101:113–117. doi:10.1016/j.vacuum.2013.07.046

[16] Pan X, Zhao X, Chen J, Bermak A, Fan Z (2015) A fast-response/recovery ZnO hierarchical nanostructure based gas

sensor with ultra-high room-temperature output response. Sens Actuat B 206:764–771. doi:10.1016/j.snb.2014.08.089

[17] Moezzi A, McDonagh AM, Cortie MB (2012) Zinc oxide particles: synthesis, properties and applications. Chem Eng J 185–186:1–22. doi:10.1016/j.cej.2012.01.076

[18] Wei A, Pan L, Huang W (2011) Recent progress in the ZnO nanostructure-based sensors. Mater Sci Eng B 176:1409–1421. doi:10.1016/j.mseb.2011.09.005

[19] Shouli B, Liangyuan C, Dianqing L, Wensheng Y, Pengcheng Y, Zhiyong L, Aifan C, Liu CC (2010) Sens Actuat B 146:129–137. doi:10.1016/j.snb.2010.02.011

[20] Septiani NLW, Yuliarto B (2016) Review—the development of gas sensor based on carbon nanotubes. J Electrochem Soc 163:B97–B106. doi:10.1149/2.0591603jes

[21] Poornajar M, Marashi P, Fatmehsari DH, Esfahani MK (2016) Synthesis of ZnO nanorods via chemical bath deposition method: the effects of physicochemical factors. Ceram Int 42:173–184. doi:10.1016/j.ceramint.2015.08.073

[22] Li Q, Bian J, Sun J, Wang J, Luo Y, Sun K, Yu D (2010) Controllable growth of well-aligned ZnO nanorod arrays by low-temperature wet chemical bath deposition method. Appl Surf Sci 256:1698–1702. doi:10.1016/j.apsusc.2009.09.097

[23] Shi Y, Wang M, Hong C, Yang Z, Deng J, Song X, Wang L, Shao J, Liu H, Ding Y (2007) Multi-junction joints network self-assembled with converging ZnO nanowires as multi-barrier gas sensor. Sens Actuat B 177:1027–1034. doi:10.1016/j.snb.2012.11.084

[24] Miller DR (2014) Nanoscale metal oxide-based heterojunctions for gas sensing: a review. Sens Actuat B 204:250–272. doi:10.1016/j.snb.2014.07.074

[25] Tyagi P, Sharma A, Tomar M, Gupta V (2016) Metal oxide catalyst assisted SnO2 thin film based SO2 gas sensor. Sens Actuat B 224:282–289. doi:10.1016/j.snb.2015.10.050

[26] Das S, Chakraborty S, Parkash O, Kumar D, Bandyopadhyay S, Samudrala SK, Sen A, Maiti HS (2008) Vanadium doped tin dioxide as a novel sulfur dioxide sensor. Talanta 75:385–389. doi:10.1016/j.talanta.2007.11.010

[27] Peng S, Wu G, Song W, Wang Q (2013) Application of flower-like ZnO nanorods gas sensor detecting decomposition products. J Nanomater 2013:1–7

[28] Li F, Li C, Zhu L, Guo W, Shen L, Wen S, Ruan S (2016) Enhanced toluene sensing performance of gold-functionalized WO3. H2O nanosheets. Sens Actuat B 223:761–767. doi:10.1016/j.snb.2015.10.005

[29] Pawar RC, Lee J-W, Patil VB, Lee CS (2013) Synthesis of multi-dimensional ZnO nanostructures in aqueous medium for the application of gas sensor. Sens Actuat B 187:323–330. doi:10.1016/j.snb.2012.11.100

[30] Boeker P, Wallenfang O, Horner G (2002) Mechanistic model of diffusion and reaction in thin sensor layers—the DIRMAS model. Sens Actuat B 83:202–208. doi:10.1016/S0925-4005(01)01041-3

[31] Yuliarto B, Kumai Y, Inagaki S, Zhou H (2009) Enhanced benzene selectivity of mesoporous silica SPV sensors by incorporating phenylene groups in the silica framework. Sens Actuat B 138:417–421. doi:10.1016/j.snb.2009.02.022